

# Scalable Fabrication of Carbon Nanomaterials by Electrochemical Dual-Electrode Exfoliation of Graphite in Hydroxide Molten Salt

Juan Yang, Kaifa Du, Liangyou Hu, and Dihua Wang\*



Cite This: *Ind. Eng. Chem. Res.* 2020, 59, 10010–10017



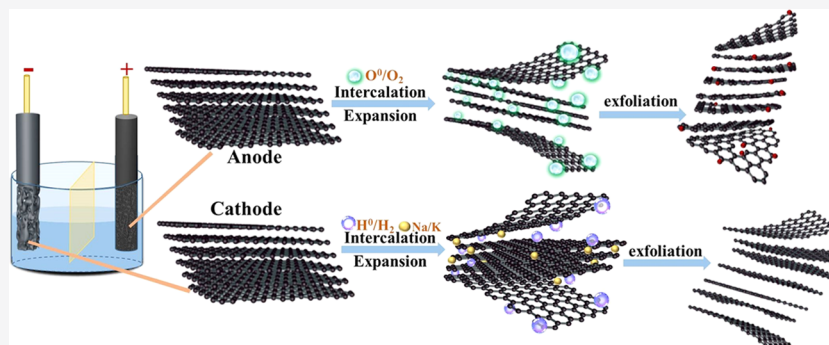
Read Online

ACCESS |

Metrics & More

Article Recommendations

Supporting Information



**ABSTRACT:** Simultaneous electroexfoliation of graphite on both cathode and anode in molten NaOH–KOH was proposed and found to be a feasible method for the mass production of carbon nanomaterials. During this electrolysis process, alkaline cations and hydroxide ions were intercalated into the bulk graphite and then discharged to generate alkaline metals and hydrogen at the cathode, and oxygen at the anode. The simultaneous intercalation on both electrodes and the escape of gas enhanced the exfoliation efficiency, leading to a high production rate of nanostructured carbon exceeding  $26.9 \text{ g h}^{-1}$ . The four to seven layers of graphene nanosheets with negligible defect ( $I_D/I_G = 0.079$ ) and low oxidation degree (C/O ratio = 20.32) were obtained through cathodic exfoliation, while the corresponding anodic exfoliation products featured more oxygen-containing functional groups (7.59%). This introduced method was beneficial for the mass production of carbon materials in a highly efficient way.

## INTRODUCTION

Since graphene exfoliation fabricated by a mechanical cleavage using adhesive tape from graphite, the preparation of carbon functional materials including graphene, graphene oxide, carbon nanotube, heterogeneous-atom-doped carbon, metal-filled carbon nanoparticle, and metallic oxide/carbon substrate by the means of graphite bulk exfoliation have gained a wide attention.<sup>1–9</sup> The layered graphite possesses strong in-plane covalent bonds and weak interlayer bonds coupled with van der Waals interactions, thus it could be easily delaminated down to thin carbon nanomaterials through the breaking of these weak bonds. Generally, there exist mechanical-based and chemical processes to exfoliate graphite. The mechanical exfoliation method mainly contains two kinds of mechanical forces. One acts to break the interlayer bonds between the interlayers of graphite directly, and the other is a shear force to slide away layer by layer.<sup>10–12</sup> For example, Zhu et al. reported gas exfoliation of graphite to expand its interlayer distance with the aid of high temperature and liquid nitrogen vaporization.<sup>13</sup> Paton et al. disclosed that high-shear mixing of graphite in exfoliating liquids composed of polymer, organic solvent, and surfactant could produce highly dispersed graphene nanosheets.<sup>14</sup> These procedures are suitable for generating high-

quality graphene. However, the concentrations of exfoliated graphene dispersions are basically below  $1 \text{ mg mL}^{-1}$ , and long-term sonication is frequently needed, which is less competitive in terms of yield and economic benefit.<sup>15</sup> For chemical exfoliation, Hummers oxidation–reduction strategy is one of the widely used exfoliation methods. This approach includes chemical oxidization of graphite, the exfoliation of graphite oxide, and the final chemical or thermal reduction of individual layers of graphene oxide. Thereby, it could cause heavy damage to the exfoliation products as well as the consumption of a vast amount of oxidants and corrosive acids.<sup>16</sup>

Another common chemical method, referred to as electrochemical exfoliation, is considered as a potentially feasible, effective, and convenient strategy to exfoliate graphite due to its simple operation, scale-up production, scalability, and product controllability.<sup>17,18</sup> During the exfoliation process,

Received: March 20, 2020

Revised: April 25, 2020

Accepted: May 5, 2020

Published: May 5, 2020



ACS Publications

anodic oxidation or cathodic reduction with a highly positive/negative charge is performed on the graphite electrode, which essentially leads the migration of various intercalants into the space between layers, inducing structural expansion and subsequent dissociation.<sup>15,18</sup> Electrochemical exfoliation in an aqueous solution has been investigated extensively. The frequently used electrolyte is mineral acids, such as H<sub>2</sub>SO<sub>4</sub>, H<sub>3</sub>PO<sub>4</sub>, HNO<sub>3</sub>, and HBF<sub>4</sub>, and inorganic salts, such as (NH<sub>4</sub>)<sub>2</sub>SO<sub>4</sub>, (NH<sub>4</sub>)<sub>2</sub>HPO<sub>4</sub>, and K<sub>2</sub>SO<sub>4</sub>.<sup>19–25</sup> Recent works also apply surfactants (e.g., sodium dodecyl sulfate and cetyltrimethylammonium bromide) as electrolytes or additives to exfoliate graphite as well as stabilize the products.<sup>8,26,27</sup> However, the conventionally exfoliated graphene products always feature large defects due to the inevitable overoxidation of graphite. For the anodic exfoliation, the continuous oxidation will lead to the degraded electrochemical intercalation and exfoliation.<sup>20</sup> Moreover, insufficient intercalants and inefficient exfoliation restrict their long-term use, and the products are difficult to obtain in large quantities. By contrast, the cathodic exfoliation, involving the utilization of ionic liquid or organic solvent that contains quaternary ammonium salt or lithium salt, is subject to the intercalation of cation into graphite cathode and could avoid the generation of defects in the exfoliation products.<sup>28–30</sup> Unfortunately, intercalation and exfoliation efficiencies are limited due to the large cations or solvated ions, which have a slow migration rate and easily break down graphite into thick pieces.<sup>31</sup> For example, Lei et al. reported that graphite cathode can be exfoliated in an ionic liquid (i.e., AlCl<sub>3</sub>/1-ethyl-3-methylimidazolium chloride) to generate few-layer graphene with only 10 mA g<sup>-1</sup> current density.<sup>29</sup>

Alternatively, electrochemical exfoliation in molten salt shows competitiveness compared with low-temperature exfoliation since molten salt electrolyte can provide a uniform heating media, high ionic conductivity, and sufficient intercalated ions.<sup>32</sup> Enhanced reactivity and promoted reaction kinetics of the electrochemical exfoliation reaction can be achieved, reflected by a current density as high as 1 A cm<sup>-2</sup> (about 1.7 A g<sup>-1</sup>).<sup>32</sup> Therefore, it makes the electrolytic conversion of graphite attractive and could offer a potential approach of a scalable preparation to harvest high-quality carbon nanomaterials.<sup>32–35</sup> It was reported that the production rate of carbon nanostructures could reach up to 10 g h<sup>-1</sup> through the cathodic polarization of the graphite rod in molten LiCl.<sup>33</sup> In this electrolytic process, lithium ions migrate to graphite cathode under the action of an electric field and subsequently intercalate into the graphite matrix to drive structural expansion, leading to the exfoliation of graphite. The resultant electrolytic carbon materials (ECMs) generally feature a high degree of crystallinity.<sup>32</sup>

In addition to the conventional alkali metal intercalation, the hydrogen-ion intercalation is another mode to implement the molten salt electrochemical exfoliation. The mechanism is based on the discharge of hydrogen ions on the polarized graphite electrode, thus generating the hydrogen gas to peel off the graphite.<sup>35,36</sup> Kamali et al. reported that low-defect graphene nanosheets ( $I_D/I_G = 0.28$ ) could be obtained in this way by adding humid Ar in a molten LiCl electrolyte to produce hydrogen ions.<sup>36</sup> Thereafter, their group successfully achieved a daily production of 200 g of high-quality graphene by directly injecting H<sub>2</sub> into the electrolyte.<sup>35</sup> These provide evidence that the molten salt electrochemical exfoliation method could be easily scaled up to produce high-quality

carbon materials. Furthermore, one of the most attractive features of this technology is that various carbon nanomaterials such as graphene, nanotubes, nanofibers, nanoparticles, nanosheets, and nanodiamonds, can be acquired by varying the electrolysis conditions.<sup>32,37–41</sup>

Nonetheless, the production of carbon nanomaterials by the molten salt electrolytic method reported so far has been performed in molten halogen salt. The ECMs are usually harvested at the cathode side through a single-ion (alkali metal ion or proton) intercalation, while the anode is consumed or generates harmful chlorine gas, resulting in energy and chemical losses and low exfoliation efficiency. Expectedly, the critical obstacle lies in the exploration of suitable intercalants that can coexist stably and intercalate into both the electrodes simultaneously. Based on this criterion, herein, we proposed a high-yield electrochemical method to achieve the simultaneous dual-electrode exfoliation through the utilization of the NaOH–KOH molten salt. The merits of this approach lie in the fact that (1) the cathodic graphite was intercalated and then exfoliated with both alkali metal and hydrogen, while the anodic graphite was exfoliated through the escape of oxygen, resulting in the whole process being more efficient and productive; (2) owing to the different intercalation reactions, the formed ECMs possess different structures on dual electrodes; (3) the intercalation species were sufficient and there was no need to consider additional introduction or conversion; (4) compared with the previous reports that were usually conducted in halide-fused salts above 600 °C, this exfoliation system was carried out at a relatively low temperature (300 °C), which could reduce the requirements of the equipment and avoid the oxidation of ECMs at the ascendant temperature; (5) this efficient procedure produced high-quality ECMs with a high production rate exceeding 26.9 g h<sup>-1</sup> in laboratory fabrication, and the obtained graphene nanosheets had negligible defect ( $I_D/I_G = 0.079$ ) and low oxidation degree (C/O ratio = 20.32). Therefore, this dual-electrode molten salt exfoliation technology has broad prospects in industrial production to produce high-quality carbon materials meeting various application demands.

## EXPERIMENTAL SECTION

**Electrochemical Exfoliation.** A graphite crucible (80 mm inner diameter and 200 mm height) with an alumina plate diaphragm was made into a dual-electrolysis cell. The Al<sub>2</sub>O<sub>3</sub> plate was positioned across the inner wall of the crucible, leaving 20 mm gaps from the bottom to conduct electrolyte between cathode and anode room. The crucible was filled with 500 g of anhydrous NaOH–KOH powders (molar ratio = 48.5:51.5) and then sealed in a stainless steel reactor heated by a tube furnace. Subsequently, the temperature of the steel reactor was slowly raised to 300 °C in an inert atmosphere of argon. Mixture hydroxide salt was melted, and its liquid level was about 50 mm, which was enough to cover the bottom of the Al<sub>2</sub>O<sub>3</sub> plate. Galvanostatic electrolysis was performed using a two-electrode system in which two graphite rods with a density of 1.75 g cm<sup>-3</sup> and a diameter of 2 cm were positioned on both sides of the partition. One of them was cathodic polarization, while the other served as an anode. The schematic drawing of the experimental setup is shown in Figure S1.

In the electrolysis process, the current densities were set at 0.5, 1, 5, and 8 A cm<sup>-2</sup>, respectively, and the effluent gas from the reactor was monitored by a gas analyzer (Nanjing Aiyi Technology Co. Ltd., China), which could recognize CO,

$\text{CO}_2$  and  $\text{O}_2$ . After the termination of electrolysis, exfoliation products floating on the liquid surface on both sides of the partition were collected through a mesh iron and then naturally cooled to room temperature under flowing argon. Afterward, the obtained products were thoroughly washed and finally dried under vacuum. The products were denoted as the cathodic electrolytic carbon material (C-ECM-X) and the anodic electrolytic carbon material (A-ECM-X), where X represents the applied current density.

Linear sweep voltammetry (LSV) studies were carried out on a model CHI 1140C electrochemical workstation (Shanghai Chenhua Instrument, China). A eutectic  $\text{NaOH}-\text{KOH}$  melt was used as an electrolyte. A conventional three-electrode system was adopted, including an Ag wire as a quasi-reference electrode and two graphite rods of 5 mm diameter contacted with stainless steel as a working electrode and a counter electrode, respectively. The apparatus diagram of the electrochemical measurement was similar to the electrolytic system (Figure S1), except that an additional reference electrode was added.

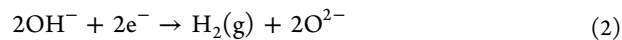
**Characterization.** The morphologies of ECMs were examined by field emission scanning electron microscopy (SEM, ZEISS, Germany) and transmission electron microscopy (TEM, JEMe2100, Japan). X-ray diffraction (XRD) patterns were collected from a PANalytical X'Pert Pro diffractometer (Holland) using  $\text{Cu K}\alpha$  radiation (40 kV, 40 mA) with a Ni filter. X-ray photoelectron spectroscopy (XPS) characterizations were recorded with a ThermoFisher ESCALAB 250Xi X-ray photoelectron spectrometer with  $\text{Al K}\alpha$  X-ray radiation for excitation. Raman spectra were recorded using a laser confocal Raman microspectroscopy (Renishaw RM1000, U.K.) with an excitation wavelength at 514.5 nm from an  $\text{Ar}^+$  laser. The thermodynamic data of the selected reactions were calculated using a commercial software HSC 6.0.

## RESULTS AND DISCUSSION

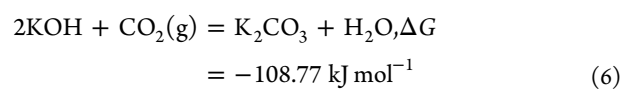
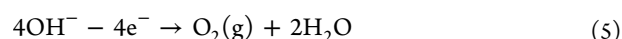
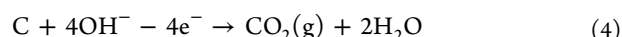
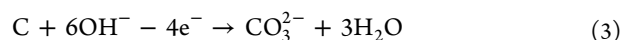
Unlike the commonly used chloride molten salt, mixed  $\text{NaOH}-\text{KOH}$  molten salt with a low eutectic point ( $170^\circ\text{C}$ ) was used in this work, so that the total electrolysis processes were carried out at a relatively low temperature ( $300^\circ\text{C}$ ). At this temperature, the involved electrochemical reactions and the corresponding thermodynamic data are all listed in Table 1. To compare the potential of different reactions, a standard anodic reaction of  $\text{O}_2$  evolution or a cathodic reaction of alkali metal precipitation was respectively assigned as a reference. Thermodynamically, alkali metal

electrodeposition and  $\text{H}_2$  generation occurred almost simultaneously on the cathode. At the anode side, the graphite was more favorable to be oxidized to form carbonate,  $\text{CO}_2$ , and CO in the order, and subsequently generated  $\text{O}_2$  from the discharge of  $\text{OH}^-$ .

LSVs were recorded to investigate the electrode process of graphite in molten  $\text{NaOH}-\text{KOH}$  (Figure 1). When the potential was scanned from an open-circuit potential to  $-2.0\text{ V}$ , metal ions and hydroxide ions were absorbed on the surface of graphite, resulting in alkaline metal deposition and  $\text{H}_2$  evolution reaction (Figure 1A). As the potential increased, the cathode polarization was enhanced, inducing more intense electrolytic reactions. The corresponding half-reaction equations were expressed as follows



Accordingly, when the positive polarization was applied at the graphite electrode, a large number of hydroxide ions showed a positive migration under the force of an electric field. Combined with the thermodynamic calculations, it could be speculated that the oxidation peak a1 corresponded to the oxidation of graphite to form  $\text{CO}_3^{2-}$  (eq 3) and a2 represented the dissolution of gas (Figure 1B). To confirm this point, potentiostatic electrolysis was conducted at different working potentials. It was found that there was no visual bubble production, except that the applied potential exceeded  $1.7\text{ V}$  (vs Ag quasi-reference). Moreover, the releasing gas was recognized as  $\text{O}_2$  only, and the oxygen content increased with the enhanced polarization (Figure S2A). No  $\text{CO}_2$  or CO was detected even at high polarization, which was contrary to the trends of the gas formation (Table 1). The main reason was that once  $\text{CO}_2$  was produced at the anode, it was quickly captured by a molten salt to form carbonate spontaneously (eqs 6 and 7). As for the lack of CO, it was mainly due to the slow kinetics in the real electrolysis at such a low temperature. Therefore, the reactions occurring at the anode side were described as follows



After 1 min electrolysis at  $0.5\text{ A cm}^{-2}$ , both graphite electrodes were obviously eroded. The bottom of the cathode became rough, and the anode displayed extraordinary indentations. Most indentations were nearly spherical, and their edges were in the shape of strips mainly due to the different diffusion paths of the formed gas (Figure S2B,C). For comparison, the morphologies of the raw graphite and the used graphite cathode were also recorded. As shown in Figure 2, the feed material displayed a typical flake structure, which was smooth

**Table 1. Thermodynamic Data of the Electrolytic Reactions in  $\text{NaOH}-\text{KOH}$  Molten Salt at  $300^\circ\text{C}$**

reactions	$\Delta G$ (kJ mol $^{-1}$ )	$\Delta E$ (V)
$6\text{KOH} + \text{C} = 4\text{K} + \text{K}_2\text{CO}_3 + 3\text{H}_2\text{O}$	457.26	1.18
$6\text{NaOH} + \text{C} = 4\text{Na} + \text{Na}_2\text{CO}_3 + 3\text{H}_2\text{O}$	474.97	1.23
$4\text{KOH} + \text{C} = 4\text{K} + 2\text{H}_2\text{O} + \text{CO}_2(\text{g})$	566.03	1.46
$4\text{NaOH} + \text{C} = 4\text{Na} + 2\text{H}_2\text{O} + \text{CO}_2(\text{g})$	567.90	1.47
$2\text{KOH} + \text{C} = 2\text{K} + \text{H}_2\text{O} + \text{CO}(\text{g})$	318.49	1.65
$2\text{NaOH} + \text{C} = 2\text{Na} + \text{H}_2\text{O} + \text{CO}(\text{g})$	319.43	1.66
$4\text{KOH} = 4\text{K} + 2\text{H}_2\text{O} + \text{O}_2(\text{g})$	961.12	2.49
$4\text{NaOH} = 4\text{Na} + 2\text{H}_2\text{O} + \text{O}_2(\text{g})$	962.99	2.50
$8\text{NaOH} = 4\text{Na}_2\text{O} + 2\text{H}_2\text{O} + 2\text{H}_2(\text{g}) + \text{O}_2(\text{g})$	967.06	2.51
$8\text{KOH} = 4\text{K}_2\text{O} + 2\text{H}_2\text{O} + 2\text{H}_2(\text{g}) + \text{O}_2(\text{g})$	1189.51	3.08

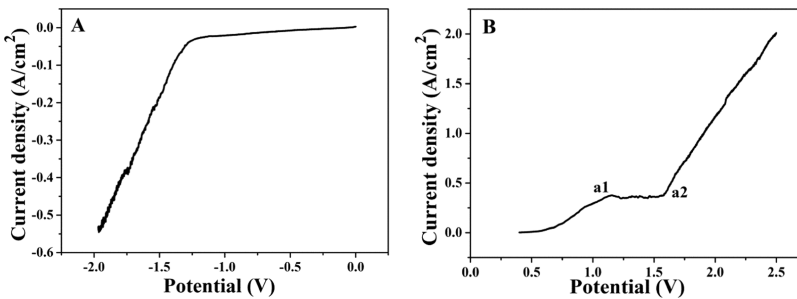


**Figure 1.** Cathode polarization curve (A) and anode polarization curve (B) of the graphite electrodes (vs Ag quasi-reference) in the eutectic NaOH–KOH melt. Sweep rate = 5 mV s<sup>-1</sup>, T = 300 °C.

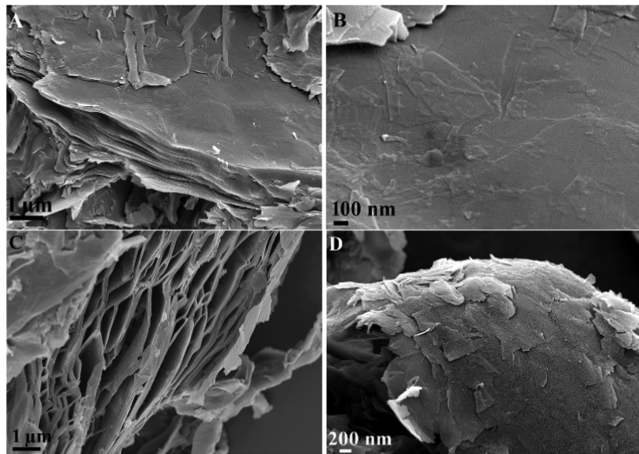


**Figure 2.** SEM images of pristine graphite (A, B) and graphite cathode after electrolysis at 0.5 A cm<sup>-2</sup> (C, D) in different perspectives.

and stacked tightly (Figure 2A,B). However, the graphite rod after electrolysis showed expansion and had a distinct interval space. The graphite surface was broken and cracked into unfallen fragments (Figure 2C,D).

Moreover, after continuing electrolysis for a longer time, the graphite rods were eroded more seriously (Figure S3). At 0.5 A cm<sup>-2</sup>, the cathode was eroded into a cone due to the unique electric-field distribution. Herein, the exfoliation mass was about 15.9 g. When the current density was increased to 1 A cm<sup>-2</sup>, the immersion portion of graphite was eroded

completely within 37 min and the exfoliation product was increased to 19.2 g. Correspondingly, under the action of positive polarization, the anode became thinner and its surface featured irregular pits. The A-ECMs, with a mass of about 0.19 and 0.30 g, were obtained by the oxygen exfoliation and the scour of carbon dioxide at 0.5 and 1 A cm<sup>-2</sup>, respectively. In fact, the volume expansion of graphite aroused by the intercalation effect might lead to an actually low yield of A-ECMs. The electrolysis energy consumption in NaOH–KOH molten salt was about 1.55 kW h kg<sup>-1</sup>, which was much lower than that of reported LiCl molten salt (4.1 kW h kg<sup>-1</sup>).<sup>9</sup> In addition, the total exfoliation rates were calculated as 26.9 and 31.7 g h<sup>-1</sup>, respectively, which were both higher than that of other electrochemical graphite peeling systems (Table 2). Such high exfoliation rates were attributed to the simultaneous intercalation on both electrodes, and the synergistic effect of ions co-intercalation and gas escape.

Based on the above phenomena, an electrochemical exfoliation mechanism was proposed and is illustrated in Figure 3. During the cathodic intercalation process, metal ion and OH<sup>-</sup> around graphite were inserted into graphite layers and then reduced when the polarization current was applied, resulting in enlarged gaps between the neighboring layers of graphite. The expansion caused the alkali cation and OH<sup>-</sup> to diffuse far into the graphite bulk easily.<sup>36,42</sup> After that, the graphite sheets started to exfoliate when the mechanical stress produced by the intercalation species was too high for the graphite matrix to accommodate.<sup>33</sup> Besides, the release of gas inside the adjacent layers also accelerated the splitting of graphite to fracture into small-size products.<sup>10</sup> During the

**Table 2. Comparison of Electrolytic Parameter, Production Rate, C/O Ratio, and Defect of Exfoliation Product Prepared by Electrochemical Exfoliation**

synthetic methods	electrolytic parameter	production rate (g h <sup>-1</sup> )	C/O ratio	I <sub>D</sub> /I <sub>G</sub>	ref
EAE <sup>a</sup> : 0.1 M H <sub>2</sub> SO <sub>4</sub>	10 V	~4.2	12.3	0.4	45
EAE: 0.1 M (NH <sub>4</sub> ) <sub>2</sub> SO <sub>4</sub>	10 V	~10.9	17.2	0.25	46
DEE <sup>b</sup> : H <sub>2</sub> SO <sub>4</sub> /melamine	20 V	1.5	26.17	0.20–0.54	20
DEE: 0.1 M TBAClO <sub>4</sub> /PC <sup>c</sup>	5 V	25	A <sup>d</sup> : 18.42 C <sup>e</sup> : 21.37	A: 0.071 C: 0.079	31
ECE <sup>f</sup> : LiCl (770 °C)	1 A cm <sup>-2</sup>	10			33
ECE: LiCl (800 °C)	33 A	20	21.02	0.286	36
ECE: NaCl/H <sub>2</sub> (900 °C)	35 A		32.6	0.833	35
DEE: NaOH–KOH (300 °C)	0.5 A cm <sup>-2</sup>	26.9	A: 12.18 C: 20.32	A: 0.216 C: 0.079	this work
	1 A cm <sup>-2</sup> (9.42 A)	31.7		A: 0.102 C: 0.182	

<sup>a</sup>Electrochemical anodic exfoliation (EAE). <sup>b</sup>Dual-electrode exfoliation (DEE). <sup>c</sup>Tetrabutylammonium perchlorate/propylene carbonate. <sup>d</sup>Anode (A). <sup>e</sup>Cathode (C). <sup>f</sup>Electrochemical cathodic exfoliation (ECE).

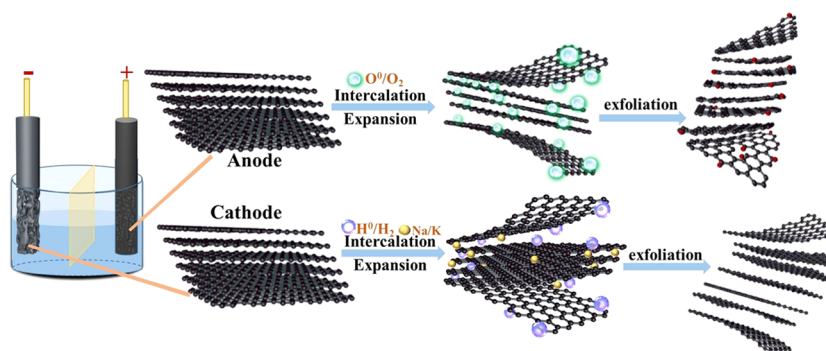


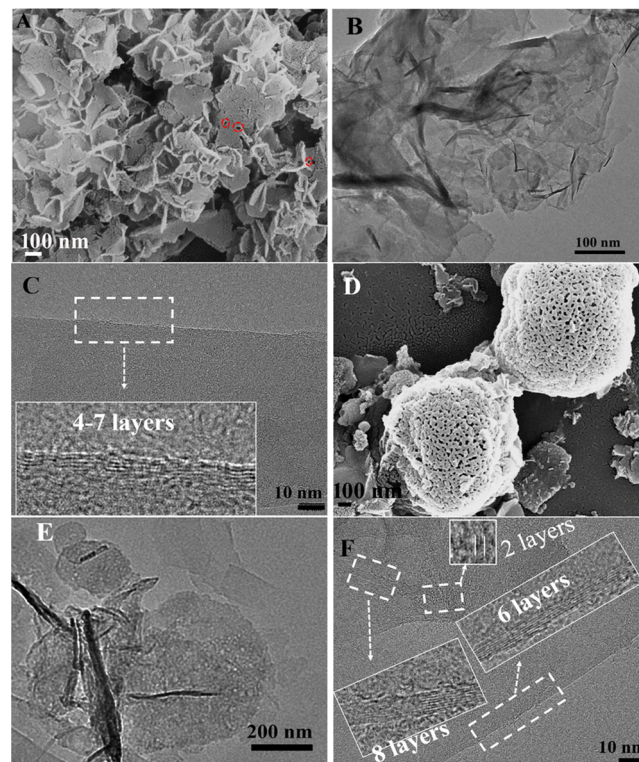
**Figure 3.** Illustration of the mechanism involved in the preparation of ECMs from graphite in molten NaOH–KOH.

intercalation process, the intercalation species were prior to the attack, the edge sites, and grain boundaries of graphite because the crystallite surface and boundary possessing larger interlamellar spacing and lower steric hindrance were vulnerable to attack. As the current density increased, the driving force was enhanced, inducing a more dramatic exfoliation. As a result, more cathodic products were obtained.

Meanwhile, at the anode side, a mass of  $\text{OH}^-$  migrated to the graphite surface under the action of the electric field and the high concentration of  $\text{OH}^-$  with an ionic radius of 0.137 nm was easily inserted into the graphite matrix to expand its lattice distance.<sup>43</sup> It was straightforward to confirm that the hydroxide ion could give birth to oxygen gas under positive polarization, and the eruption of gaseous bubbles formed in the expanded graphite could overwhelm the van der Waals resistance, leading to the exfoliation of graphite. In addition, a consumptive corrosion reaction in which partial graphite was inevitably oxidized to  $\text{CO}_2$  also coexisted in this exfoliation process. The generated cavitation bubbles were conducive to exposing more defective sites and facilitating the intercalation of  $\text{OH}^-$ . Besides, the defect in graphite was more readily oxidized due to the free bonded atoms, resulting in oxygen functional groups (e.g., C–O–C, C–OH, C=O) formed on A-ECMs.<sup>44</sup> Coincidentally, the oxidized graphite had good compatibility with molten salt, which contributed to accelerating the dissociation of graphite through pulling the graphite edge outward.

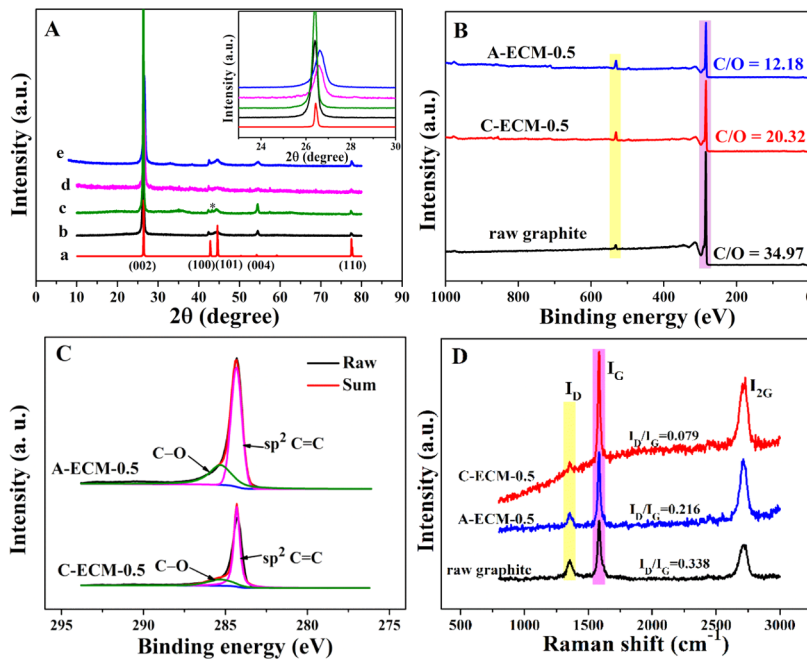
SEM and TEM were used to analyze the morphologies of ECMs (Figure 4). Unlike the bulk graphite, which possessed structured micron-size flakes, C-ECM-0.5 had clusters of graphene nanosheets with random orientation and its surface featured with numerous nanopores (marked as circles) and cracks. The nanosheets were stacked and some were folded, wrinkled to form layered clusters of four to seven sheets. The microstructure of A-ECMs was entirely different from that of the C-ECMs. The gas-driven exfoliated A-ECM-0.5 mainly existed in the form of spherical carbon particles with a nanoporous structure, which was the result of the rushing out of gas during the graphite oxidation process. Besides, a few irregular sheets also existed. The two- to eight-layer heterogeneous edge of A-ECMs can be observed in the enlarged HRTEM images.

Figure 5A describes the XRD results of the relevant materials. The characteristic peaks that correspond to the (002), (100), (101), (004), and (110) planes of the pristine graphite (curve b) still remained in the ECMs except with slight shift and broadening (curve d–e).<sup>34</sup> As can be seen, the strong feature diffraction peak (i.e., (002)) of raw graphite with



**Figure 4.** SEM images of C-ECM-0.5 (A) and A-ECM-0.5 (D). TEM and HRTEM images of C-ECM-0.5 (B, C) and A-ECM-0.5 (E, F).

a maximum at  $2\theta = 26.38^\circ$  shifted to higher values of  $2\theta = 26.57$  and  $26.62^\circ$  in A-ECM-0.5 (curve d) and C-ECM-0.5 (curve e), respectively. It corresponded to the decrease in the graphitic layer spacing  $d_{002}$  from 0.3376 nm for the raw graphite to 0.3352 and 0.3346 nm for the anode and cathode products, respectively. The obviously reduced lattice distance between the  $\text{sp}^2$ -carbon layers of the ECMs showed an increased crystalline quality of the graphitic materials, which became closer to a perfect graphite crystal. The results are in agreement with the previously reported observations.<sup>29,33</sup> Additionally, the diffraction peaks of the products were obviously broad due to the reduction in the size of crystalline domains, which was in accordance with the SEM characterization. For comparison, direct soaking of graphite without electrolysis was also conducted (curve c) in NaOH–KOH molten salt at 300 °C. Nevertheless, no visible broadening was observed, but a new signal (asterisk marked) distinguished from the raw graphite appeared, possibly assigned to the formed graphite intercalation compounds.<sup>43</sup> The small-angle



**Figure 5.** (A) XRD patterns of simulated graphite (a), raw graphite electrode (b), graphite powder after soaking (c), A-ECM-0.5 (d), and C-ECM-0.5 (e). (B) Survey XPS data of raw graphite and electrolytic products obtained at  $0.5 \text{ A cm}^{-2}$ . (C) High-resolution C 1s XPS data of electrolytic products obtained at  $0.5 \text{ A cm}^{-2}$ . (D) Raman spectra of the pristine graphite, A-ECM-0.5, and C-ECM-0.5. The inset was the locally enlarged XRD patterns of all samples.

shift of the soaking graphite indirectly confirmed the intercalation of mobilizable  $\text{OH}^-$ , thus inducing the interlayer gap expansion.

In addition, the content of the constituent element in ECM-0.5 was also determined by XPS (Figure 5B). The oxygen percentage of C-ECM-0.5 was 4.69%, which was a slight increase of over 2.78% for pure graphite. It is possibly due to more terminated edge sites and enlarged exposure areas of exfoliation products, thus creating accrescent reactivity. The content of oxygen in A-ECM-0.5 (7.59%) was higher than that in C-ECM-0.5, which was largely due to the oxidation of graphite during positive polarization, resulting in the exfoliation products modifying many oxygen-containing functional groups. The index C/O atomic ratios were calculated as 12.18 and 20.32 for A-ECM-0.5 and C-ECM-0.5, respectively. Both of them were much larger than those of the other electrochemical exfoliation methods (Table 2), indicating the high quality of products harvested from  $\text{NaOH}-\text{KOH}$  molten salt electrolysis. Meanwhile, the chemical state of carbon in ECMs was analyzed (Figure 5C). The peaks fitting the C 1s XPS spectra of C-ECM-0.5 and A-ECM-0.5 both included two chemical bonds, which mainly consisted of sp<sup>2</sup>-hybridized graphitic carbon (284.3 eV) and C–O (285.4 eV). Consistent with the oxygen content, the proportion of C–O in A-ECM-0.5 was much higher.

To further evaluate the graphitization degree of products, Raman spectroscopy characterization was investigated (Figure 5D). The D-band near  $1355 \text{ cm}^{-1}$  was attributed to structural defects and partially disordered structure of carbon, and the G-band at  $1581 \text{ cm}^{-1}$  was associated with in-plane vibration of the sp<sup>2</sup> carbon atoms. The D-band was remarkably weak in exfoliation samples. The  $I_D/I_G$  ratio, an index to evaluate the density of edge defects in carbon-based materials,<sup>47</sup> was calculated as 0.216 and 0.079 for A-ECM-0.5 and C-ECM-0.5, which was lower than for the reduced graphite oxide (about

1.1–1.5) and the electroexfoliation graphene (0.4) in  $\text{H}_2\text{SO}_4$ ,<sup>45,48</sup> indicating the low defect of ECMs gained from this molten salt electrochemical exfoliation method. The peak at about  $2720 \text{ cm}^{-1}$  was assigned to a two-dimensional (2D) band, which was extremely sensitive to the number of layers. The half-peak width of the 2D peak in ECMs-0.5 was between 62 and  $65 \text{ cm}^{-1}$ , suggesting that the products were comprised of more than five layers of graphene.

The electrolytic products obtained at higher current densities were also characterized to investigate its structure and composition changes (Figures S4–S7). Different product morphologies were apparently observed. C-ECM-1 exhibited a mixed morphology including a cluster of bonded short sticks and few stacked carbon particles, and A-ECM-1 was a large lamellar structure featured with rough surfaces and crevices. The corresponding  $I_D/I_G$  ratio was 0.182 and 0.102, respectively (Figure S5). When the cathodic current density was up to  $5 \text{ A cm}^{-2}$ , large graphite fragments, seemingly from the damage of the graphite body, were formed. It could be ascribed to the ultrafast reduction rate that led to excessive liquid sodium and potassium accumulating in the near-surface region of the electrode. As the liquid metal did not wet the graphite well, the mass transfer of ions and the intercalation process were both slowed down. At the same time, the covering liquid metal damaged the graphite body and generated the macroscopic pieces. The measured high  $I_D/I_G$  ratio (0.238) further confirmed its relatively low quality (Figure S6). According to the variation trends of  $I_D/I_G$  values, it can be concluded that the defect density of C-ECMs increased with the enhanced cathodic polarization; however, all ECMs possessed lower defect than the raw graphite. As electrolysis is conducted at  $8 \text{ A cm}^{-2}$ , the graphite anode broke into stacked grains with a narrow size distribution of 30–50 nm. At such a high anodic polarization, the side reactions became more severe, and the oxygen content of A-ECM-8

increased to 40.22%. The curves of C 1s region of A-ECM-8 could be deconvoluted into four peaks (Figure S7), corresponding to the  $\text{sp}^2$ -hybridized graphitic carbon (284.1 eV),  $\text{sp}^3$  C–C (284.8 eV), C–O (285.9 eV), and C=O (289.2 eV), respectively, giving the signal that A-ECM may feature multiple functional groups such as carboxyl, lactone, and hydroxyl groups.<sup>49</sup> From these results, it can be concluded that the direct conversion of graphite into carbon materials with different compositions and microstructures could be achieved through the electrochemical exfoliation in NaOH–KOH molten salt and also anticipated that the quality of exfoliation products would be further improved through a fine-controlling electrolytic parameter.

## CONCLUSIONS

In summary, a facile, scalable, and high-efficient strategy for simultaneous electrochemical exfoliation of dual graphite electrodes in NaOH–KOH molten salt was demonstrated. Owing to the multispecies co-intercalated exfoliation on both anode and cathode, the whole exfoliation process offered a remarkable production rate exceeding 26.9 g h<sup>-1</sup>, which was significantly higher than that of other reported electro-exfoliation methods. In addition, exfoliation products with different structures could be harvested by controlling the polarization intensity and direction. It was found that defects in C-ECMs tended to increase with growing cathodic polarization in the range of 0.5–5 A cm<sup>-2</sup>, and the oxygen content of A-ECMs possessing more oxygen-containing functional groups than the C-ECMs would further ascend with enhanced polarization. Therefore, this strategy provides a promising route for the large-scale production of various nanostructured carbon materials.

## ASSOCIATED CONTENT

### Supporting Information

The Supporting Information is available free of charge at <https://pubs.acs.org/doi/10.1021/acs.iecr.0c01430>.

Schematic diagram of the electrolysis experimental apparatus; O<sub>2</sub> monitoring curves of the electrolysis process; digital photos of the used graphite electrodes; SEM images of ECMs-1, C-ECM-5, and A-ECM-8; Raman spectrum of ECMs-1 and C-ECM-5; and C 1s XPS data of A-ECM-8 ([PDF](#))

## AUTHOR INFORMATION

### Corresponding Author

Dihua Wang – School of Resource and Environmental Sciences, International Cooperation Base for Sustainable Utilization of Resources and Energy in Hubei Province, Wuhan University, Wuhan 430072, Hubei, P. R. China; [orcid.org/0000-0003-2364-8718](https://orcid.org/0000-0003-2364-8718); Phone: 86-27-68774216; Email: [wangdh@whu.edu.cn](mailto:wangdh@whu.edu.cn); Fax: 86-27-68775799

### Authors

Juan Yang – School of Resource and Environmental Sciences, International Cooperation Base for Sustainable Utilization of Resources and Energy in Hubei Province, Wuhan University, Wuhan 430072, Hubei, P. R. China

Kaifa Du – School of Resource and Environmental Sciences, International Cooperation Base for Sustainable Utilization of Resources and Energy in Hubei Province, Wuhan University, Wuhan 430072, Hubei, P. R. China

Liangyou Hu – School of Resource and Environmental Sciences, International Cooperation Base for Sustainable Utilization of Resources and Energy in Hubei Province, Wuhan University, Wuhan 430072, Hubei, P. R. China

Complete contact information is available at:  
<https://pubs.acs.org/10.1021/acs.iecr.0c01430>

### Author Contributions

The manuscript was written through contributions of all authors. All authors have given approval to the final version of the manuscript.

### Notes

The authors declare no competing financial interest.

## ACKNOWLEDGMENTS

This work was supported by the National Natural Science Foundation of China (Nos. 21673162 and 51874211) and the China Postdoctoral Science Foundation (No. 2019M652709).

## REFERENCES

- (1) Lavin-Lopez, M. P.; Valverde, J. L.; Sanchez-Silva, L.; Romero, A. Solvent-based exfoliation via sonication of graphitic materials for graphene manufacture. *Ind. Eng. Chem. Res.* **2016**, *55*, 845–855.
- (2) Matsumoto, M.; Saito, Y.; Park, C.; Fukushima, T.; Aida, T. Ultrahigh-throughput exfoliation of graphite into pristine ‘single-layer’ graphene using microwaves and molecularly engineered ionic liquids. *Nat. Chem.* **2015**, *7*, 730–736.
- (3) Cai, M.; Thorpe, D.; Adamson, D. H.; Schniepp, H. C. Methods of graphite exfoliation. *J. Mater. Chem.* **2012**, *22*, 24992–25002.
- (4) Gondosiwanto, R.; Lu, X.; Zhao, C. Preparation of metal-free nitrogen-doped graphene via direct electrochemical exfoliation of graphite in ammonium nitrate. *Aust. J. Chem.* **2015**, *68*, 830–835.
- (5) Lu, X.; Zhao, C. Controlled electrochemical intercalation, exfoliation and in situ nitrogen doping of graphite in nitrate-based protic ionic liquids. *Phys. Chem. Chem. Phys.* **2013**, *15*, 20005–20009.
- (6) Zhang, W.; Zeng, Y.; Xiao, N.; Hng, H. H.; Yan, Q. One-step electrochemical preparation of graphene-based heterostructures for Li storage. *J. Mater. Chem.* **2012**, *22*, 8455–8461.
- (7) Das Gupta, R.; Schwandt, C.; Fray, D. J. Preparation of tin-filled carbon nanotubes and nanoparticles by molten salt electrolysis. *Carbon* **2014**, *70*, 142–148.
- (8) Nurhafizah, M.; Suriani, A.; Mohamed, A.; Soga, T. Effect of voltage applied for graphene oxide/latex nanocomposites produced via electrochemical exfoliation and its application as conductive electrodes. *Diamond Relat. Mater.* **2020**, *101*, No. 107624.
- (9) Dimitrov, A. T.; Chen, G. Z.; Kinloch, I. A.; Fray, D. J. A feasibility study of scaling-up the electrolytic production of carbon nanotubes in molten salts. *Electrochim. Acta* **2002**, *48*, 91–102.
- (10) Zhang, Z.; Jin, H.; Miao, X.; Ju, T.; Li, Y.; Ji, J. Gas-driven exfoliation for producing high-quality graphene. *Chem. Commun.* **2019**, *55*, 7749–7751.
- (11) Karikalan, N.; Elavarasan, M.; Yang, T. C. Effect of cavitation erosion in the sonochemical exfoliation of activated graphite for electrocatalysis of acetbutolol. *Ultrason. Sonochem.* **2019**, *56*, 297–304.
- (12) Yang, H.; Li, H.; Zhai, J.; Sun, L.; Yu, H. Simple synthesis of graphene oxide using ultrasonic cleaner from expanded graphite. *Ind. Eng. Chem. Res.* **2014**, *53*, 17878–17883.
- (13) Wu, P.; He, J.; Chen, L.; Wu, Y.; Li, H.; Zhu, H.; Li, H.; Zhu, W. Few-layered graphene via gas-driven exfoliation for enhanced supercapacitive performance. *J. Energy Chem.* **2018**, *27*, 1509–1515.
- (14) Paton, K. R.; Varrla, E.; Backes, C.; Smith, R. J.; Khan, U.; O'Neill, A.; Boland, C.; Lotya, M.; Istrate, O. M.; King, P. Scalable production of large quantities of defect-free few-layer graphene by shear exfoliation in liquids. *Nat. Mater.* **2014**, *13*, 624.
- (15) Abdelkader, A.; Cooper, A.; Dryfe, R.; Kinloch, I. How to get between the sheets: a review of recent works on the electrochemical

- exfoliation of graphene materials from bulk graphite. *Nanoscale* **2015**, *7*, 6944–6956.
- (16) Xian, H.; Peng, T.; Sun, H.; Wang, J. Preparation of graphene nanosheets from microcrystalline graphite by low-temperature exfoliated method and their supercapacitive behavior. *J. Mater. Sci.* **2015**, *50*, 4025–4033.
- (17) Shi, P. C.; Lin, M.; Zheng, H.; He, X. D.; Xue, Z. M.; Xiang, H. F.; Chen, C. H. Effect of propylene carbonate-Li<sup>+</sup> solvation structures on graphite exfoliation and its application in Li-ion batteries. *Electrochim. Acta* **2017**, *247*, 12–18.
- (18) Yang, S.; Ricciardulli, A. G.; Liu, S.; Dong, R.; Lohe, M. R.; Becker, A.; Squillaci, M. A.; Samori, P.; Müllen, K.; Feng, X. Ultrafast delamination of graphite into high-quality graphene using alternating currents. *Angew. Chem., Int. Ed.* **2017**, *56*, 6669–6675.
- (19) Xia, Z.; Bellani, V.; Sun, J.; Palermo, V. Electrochemical exfoliation of graphite in H<sub>2</sub>SO<sub>4</sub>, Li<sub>2</sub>SO<sub>4</sub> and NaClO<sub>4</sub> solutions monitored in-situ by Raman microscopy and spectroscopy. *Faraday Discuss.* **2020**, DOI: [10.1039/C9FD00123A](https://doi.org/10.1039/C9FD00123A).
- (20) Chen, C.-H.; Yang, S.-W.; Chuang, M.-C.; Woon, W.-Y.; Su, C.-Y. Towards the continuous production of high crystallinity graphene via electrochemical exfoliation with molecular in situ encapsulation. *Nanoscale* **2015**, *7*, 15362–15373.
- (21) Zhao, X.; Li, H.; Han, F.; Dai, M.; Sun, Y.; Song, Z.; Han, D.; Niu, L. Electrochemical exfoliation of graphene as an anode material for ultra-long cycle lithium ion batteries. *J. Phys. Chem. Solids* **2020**, *139*, No. 109301.
- (22) Campéon, B. D. L.; Akada, M.; Ahmad, M. S.; Nishikawa, Y.; Gotoh, K.; Nishina, Y. Non-destructive, uniform, and scalable electrochemical functionalization and exfoliation of graphite. *Carbon* **2020**, *158*, 356–363.
- (23) Parvez, K.; Wu, Z.-S.; Li, R.; Liu, X.; Graf, R.; Feng, X.; Müllen, K. Exfoliation of graphite into graphene in aqueous solutions of inorganic salts. *J. Am. Chem. Soc.* **2014**, *136*, 6083–6091.
- (24) Sharif, F.; Zeraati, A. S.; Ganjeh-Anzabi, P.; Yasri, N.; Perez-Page, M.; Holmes, S. M.; Sundararaj, U.; Trifkovic, M.; Roberts, E. P. Synthesis of a high-temperature stable electrochemically exfoliated graphene. *Carbon* **2020**, *157*, 681–692.
- (25) Lowe, S. E.; Shi, G.; Zhang, Y.; Qin, J.; Jiang, L.; Jiang, S.; Al-Mamun, M.; Liu, P.; Zhong, Y. L.; Zhao, H. The role of electrolyte acid concentration in the electrochemical exfoliation of graphite: Mechanism and synthesis of electrochemical graphene oxide. *Nano Mater. Sci.* **2019**, *1*, 215–223.
- (26) Kakaei, K. One-pot electrochemical synthesis of graphene by the exfoliation of graphite powder in sodium dodecyl sulfate and its decoration with platinum nanoparticles for methanol oxidation. *Carbon* **2013**, *51*, 195–201.
- (27) Kakaei, K.; Hasanpour, K. Synthesis of graphene oxide nanosheets by electrochemical exfoliation of graphite in cetyltrimethylammonium bromide and its application for oxygen reduction. *J. Mater. Chem. A* **2014**, *2*, 15428–15436.
- (28) Wang, J.; Manga, K. K.; Bao, Q.; Loh, K. P. High-yield synthesis of few-layer graphene flakes through electrochemical expansion of graphite in propylene carbonate electrolyte. *J. Am. Chem. Soc.* **2011**, *133*, 8888–8891.
- (29) Lei, H.; Tu, J.; Yu, Z.; Jiao, S. Exfoliation mechanism of graphite cathode in ionic liquids. *ACS Appl. Mater. Interfaces* **2017**, *9*, 36702–36707.
- (30) Abdelkader, A. M.; Kinloch, I. A.; Dryfe, R. A. Continuous electrochemical exfoliation of micrometer-sized graphene using synergistic ion intercalations and organic solvents. *ACS Appl. Mater. Interfaces* **2014**, *6*, 1632–1639.
- (31) Zhang, Y.; Xu, Y. Simultaneous electrochemical dual-electrode exfoliation of graphite toward scalable production of high-quality graphene. *Adv. Funct. Mater.* **2019**, *29*, No. 1902171.
- (32) Rezaei, A.; Kamali, A. R. Green production of carbon nanomaterials in molten salts, mechanisms and applications. *Diamond Relat. Mater.* **2018**, *83*, 146–161.
- (33) Kamali, A. R.; Fray, D. J. Towards large scale preparation of carbon nanostructures in molten LiCl. *Carbon* **2014**, *77*, 835–845.
- (34) Kamali, A. R.; Fray, D. J. Molten salt corrosion of graphite as a possible way to make carbon nanostructures. *Carbon* **2013**, *56*, 121–131.
- (35) Kamali, A. R. Scalable fabrication of highly conductive 3D graphene by electrochemical exfoliation of graphite in molten NaCl under Ar/H<sub>2</sub> atmosphere. *J. Ind. Eng. Chem.* **2017**, *52*, 18–27.
- (36) Kamali, A. R.; Fray, D. J. Large-scale preparation of graphene by high temperature insertion of hydrogen into graphite. *Nanoscale* **2015**, *7*, 11310–11320.
- (37) Kamali, A. R.; Fray, D. Electrochemical interaction between graphite and molten salts to produce nanotubes, nanoparticles, graphene and nanodiamonds. *J. Mater. Sci.* **2016**, *51*, 569–576.
- (38) Kamali, A. R.; Feighan, J.; Fray, D. J. Towards large scale preparation of graphene in molten salts and its use in the fabrication of highly toughened alumina ceramics. *Faraday Discuss.* **2016**, *190*, 451–470.
- (39) Kamali, A. R.; Fray, D. J. Preparation of nanodiamonds from carbon nanoparticles at atmospheric pressure. *Chem. Commun.* **2015**, *51*, 5594–5597.
- (40) Kamali, A. R.; Fray, D. J. A possible scalable method for the synthesis of Sn-containing carbon nanostructures. *Mater. Today Commun.* **2015**, *2*, e38–e48.
- (41) Kamali, A. R.; Schwandt, C.; Fray, D. J. On the oxidation of electrolytic carbon nanomaterials. *Corros. Sci.* **2012**, *54*, 307–313.
- (42) Kamali, A. R. Eco-friendly production of high quality low cost graphene and its application in lithium ion batteries. *Green Chem.* **2016**, *18*, 1952–1964.
- (43) Miyazaki, K.; Iizuka, A.; Mikata, K.; Fukutsuka, T.; Abe, T. Acceptor-type hydroxide graphite intercalation compounds electrochemically formed in high ionic strength solutions. *Chem. Commun.* **2017**, *53*, 10034–10037.
- (44) Mao, M.; Wang, M.; Hu, J.; Lei, G.; Chen, S.; Liu, H. Simultaneous electrochemical synthesis of few-layer graphene flakes on both electrodes in protic ionic liquids. *Chem. Commun.* **2013**, *49*, 5301–5303.
- (45) Parvez, K.; Li, R.; Puniredd, S. R.; Hernandez, Y.; Hinkel, F.; Wang, S.; Feng, X.; Müllen, K. Electrochemically exfoliated graphene as solution-processable, highly conductive electrodes for organic electronics. *ACS Nano* **2013**, *7*, 3598–3606.
- (46) Parvez, K.; Wu, Z.-S.; Li, R.; Liu, X.; Graf, R.; Feng, X.; Müllen, K. Exfoliation of graphite into graphene in aqueous solutions of inorganic salts. *J. Am. Chem. Soc.* **2014**, *136*, 6083–6091.
- (47) Zhao, M.; Ma, X.; Xiao, H. Regulation of the degree of hydrogenation and electrochemical properties of graphene generated by electrochemical cathodic exfoliation by using different solvents. *Electrochim. Commun.* **2019**, *103*, 77–82.
- (48) Buglione, L.; Chng, E. L. K.; Ambrosi, A.; Sofer, Z.; Pumera, M. Graphene materials preparation methods have dramatic influence upon their capacitance. *Electrochim. Commun.* **2012**, *14*, 5–8.
- (49) Hou, H.; Banks, C. E.; Jing, M.; Zhang, Y.; Ji, X. Carbon quantum dots and their derivative 3D porous carbon frameworks for sodium-ion batteries with ultralong cycle life. *Adv. Mater.* **2015**, *27*, 7861–7866.